An Intuitive Current-Driven Passive Mixer Model Based on Switched-Capacitor Theory

Marco Sosio, Antonio Liscidini, *Member, IEEE*, and Rinaldo Castello, *Fellow, IEEE*

***Abstract*—An intuitive current-driven passive mixer model is presented. Without using complex math, it provides a signal-transfer-function/noise description of a passive mixer when used in a wireless receiver (RX) chain driven by a transconductor and loaded by a low-pass baseband (BB). Exploiting a switched-capacitor approach, the model represents a useful tool for simple hand analysis and design. The case of a 25%-duty-cycle quadrature RX chain based on a transimpedance amplifier at BB is analyzed in detail and compared with simulations, showing good accuracy.**

***Index Terms*—Current-driven passive mixers, down-conversion gain, noise figure, quadrature chain, wireless receivers (RXs).**

I. Introduction

ZERO-IF RECEIVERS (RXs) with passive mixers have become the solution of choice in recent times primarily for their low flicker noise, high linearity, and low power consumption. This has led to a large number of papers analyzing both their signal and noise behavior. However, the existing theory of passive mixers is not always intuitive. A possible reason is that, contrary to an active mixer, a passive one does not isolate RF from baseband (BB). This affects the RX signal transfer function (STF) and the noise transfer functions for both the BB and the mixer switches [1]–[9].

Passive mixers can be operated either in voltage mode or in current mode depending on the relative values of the RF and BB impedances. A general theory of passive mixers based on a Thevenin equivalent of the RF source is given in [1]. A generalized analysis of multiphase switched-series-RC networks covering both mixing and sampling and still using a Thevenin approach is described in [2].

This brief addresses current-driven passive mixers. Using a Norton equivalent of the RF source [3], it provides particularly intuitive results in the context of high, and predominantly capacitive, RF output impedance.

For such a topology, the literature has approached STF and noise from different points of view. The STF of an RX with a passive mixer has been analyzed by Mirzaei *et al.*, providing the down-conversion gain versus frequency through a current balance at the RF output of the low-noise transconductor (LNT) amplifier [4]–[6]. Circuit calculations and up-conversion to RF of the BB input impedance have been used to analyze both nonquadrature and quadrature architectures. The BB noise of a current-mode passive mixer has been first studied in a qualitative way by Redman-White and Leenaerts using a switched-capacitor (SC) approach [8]. A detailed analysis of mixer switch noise has been proposed by Chehrazi *et al.* [9] through the mathematical series expansion of a square-wave local oscillator (LO), together with an RC-filter circuit model. Both latter results, however, apply to nonquadrature architectures only.

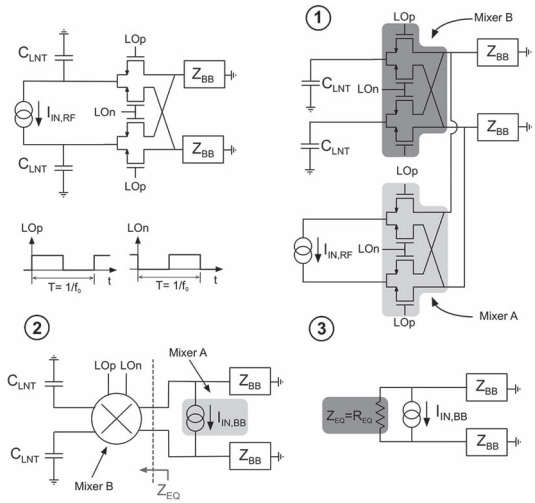

Fig. 1. 50%-D-C RX: Three-step procedure to get the SC model.

The model proposed here provides STF and noise for both single- and quadrature-chain current-driven passive mixers. The approach is based on an intuitive SC analysis that derives STF and noise from the BB point of view. While the STF description also holds for voltage-mode mixers, current-mode operation is necessary to validate the noise theory. A low-pass-BB input impedance, with a cutoff frequency below the LO frequency f_0, is always assumed. Accurate fitting is achieved if the BB cutoff frequency (for a first-order filtering) is at least one decade before f_0. This assumption is almost always satisfied in an RX chain.

This brief is organized as follows. Section II derives the STF and noise for a 50%-duty-cycle (D-C) single-chain RX. The analysis is extended to the 25%-D-C quadrature chain for STF in Section III and for BB and mixer noise in Section IV. In Section V, the model is compared with simulations for the case of an RX that uses a transimpedance amplifier (TIA) at BB. The Appendix extends the results, removing some of the simplifying assumptions.

II. 50%-D-C Single-Chain STF and Noise Model

Fig. 1 shows a fully differential implementation of a nonquadrature RX with a passive mixer. The switches are assumed ideal (i.e., $R_{\rm SW} = 0$ and the parasitic embedded in the RF and BB sections), and $Z_{\rm BB}$ is the BB input impedance. The LO is assumed to have nonoverlapping 50%-D-C square-wave

Manuscript received May 22, 2012; revised September 13, 2012; accepted November 30, 2012. Date of publication March 8, 2013; date of current version March 13, 2013. This brief was recommended by Associate Editor P. Rombouts.

M. Sosio was with the Università degli Studi di Pavia, 27100 Pavia, Italy. He is now with Marvell Italia S.R.L., 27100 Pavia, Italy (e-mail: marco.sosio1@unipv.it; marcos@marvell.com).

A. Liscidini and R. Castello are with the Università degli Studi di Pavia, 27100 Pavia, Italy (e-mail: antonio.liscidini@unipv.it; rinaldo.castello@unipv.it).

Digital Object Identifier 10.1109/TCSII.2012.2234993

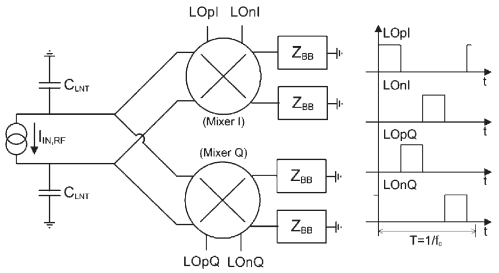

Fig. 2. 25%-D-C quadrature RX.

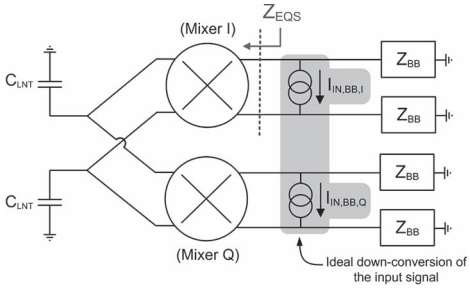

Fig. 3. Ideal down-conversion of the RF signal $I_{\mathrm{IN,RF}}$ in quadrature BB.

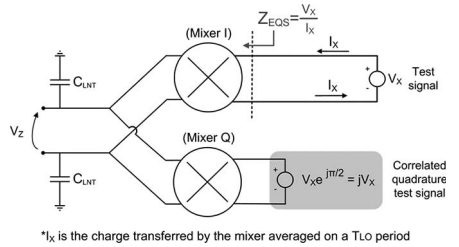

Fig. 4. Impedance calculation scheme for a quadrature-chain STF model.

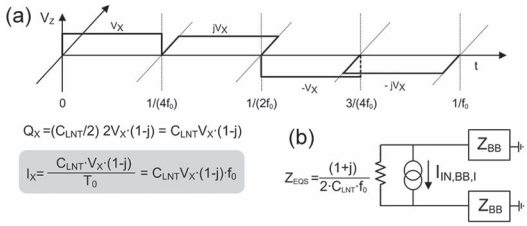

Fig. 5. (a) Differential voltage at C_{LNT} in the impedance test. (b) STF quadrature-chain model.

phases with very small rise and fall times and enough amplitude to turn on the MOS transistors with good overdrive. The LNT is modeled as a current generator $I_{\mathrm{IN,RF}}$ (phasor at frequency f_{RF}) in parallel with a capacitance C_{LNT}. For a 25%-D-C clock, the more general case of a finite resistance in parallel to C_{LNT} is also analyzed (Appendix B). An LC parallel resonant load at f_0 is not considered since, for scaled-down technologies and realizable inductances, this would require adding some extra capacitance in parallel to the parasitic, thus losing most of the benefits of such a solution [e.g., 400-fF resonation at 2 GHz (1 GHz) with 15.6 nH (62 nH), which are unpractical values in the CMOS technology].

Fig. 1 shows the three-step procedure used to derive the SC model proposed in this brief.

1) Separate the RF current generator $I_{\mathrm{IN,RF}}$ from the impedance C_{LNT} by substituting the mixer with two mixers in parallel driven by the same LO, i.e., one connected to $I_{\mathrm{IN,RF}}$ (mixer A) and the other connected to C_{LNT} (mixer B). This transformation does not modify the circuit since $R_{\mathrm{SW}} = 0$ has been assumed.
2) Down-convert $I_{\mathrm{IN,RF}}$ to BB via mixer A. The down-converted signal is the current generator $I_{\mathrm{IN,BB}}$ (Fig. 1) whose amplitude at $f_{\mathrm{RF}} - f_0$ is equal to $(2/\pi) \cdot I_{\mathrm{IN,RF}}$. Although $I_{\mathrm{IN,BB}}$ contains replicas of the RF signal around the LO harmonics, the voltage at BB is only significant at $f_{\mathrm{RF}} - f_0$ since Z_{BB} has a low-pass shape with a cutoff frequency much below f_0.
3) Replace mixer B with the equivalent impedance seen looking into its output (Z_{EQ}). For a 50% D-C, Z_{EQ} can be evaluated using a classical SC approach and corresponds to an SC resistance $R_{\mathrm{EQ}} = 1/(2C_{\mathrm{LNT}} \cdot f_0)$ [7].

The aforementioned model can produce, in a straightforward way, the mixer STF (performing a simple current partition of the down-converted current signal $I_{\mathrm{IN,BB}}$ between R_{EQ} and Z_{BB}) and the transfer functions of the BB noise sources. The noise of the mixer switches is instead obtained treating R_{EQ} as a standard noisy resistance (i.e., with a PSD equal to $4kTR_{\mathrm{EQ}}$).

Although the model has been obtained assuming that $R_{\mathrm{SW}} = 0$ and ideal LO, these assumptions can be removed, as shown in Appendix A.

III. 25%-D-C Quadrature-Chain STF Model

In the following, the derivation in Section II is extended to a quadrature RX chain with a 25%-D-C LO (Fig. 2), making the same assumptions as the 50%-D-C case. A quadrature RX with 50% D-C is not considered since it was shown to have much worse performance [5].

By using the same procedure in Section II, the RF current generator $I_{\mathrm{IN,RF}}$ is converted into two BB ones $I_{\mathrm{IN,BB},I}$ and $I_{\mathrm{IN,BB},Q}$, both with a $\sqrt{2}/\pi$ down-conversion gain (for a 25% D-C) but displaying a $\pi/2$ relative phase difference (Fig. 3).

The equivalent driving impedance Z_{EQS} seen from BB for the I (Q) path is computed as reported in Fig. 4 (the notation Z_{EQS} is used since the driving impedances for signal and noise are different). A test voltage phasor V_X is placed at the I (Q) mixer output together with a correlated one jV_X ($\pi/2$ shifted) at the Q (I) mixer output. Z_{EQS} is then evaluated as the ratio between the test generator voltage and the average current I_X flowing through it.

I_X is obtained multiplying the charge absorbed by the capacitors during the different phases of the LO period by the clock frequency. As reported in Fig. 5(a), capacitors C_{LNT} alternatively sample the test signals V_X and jV_X. This implies that the charge absorbed by the mixer every LO cycle is equal to $(1-j)V_X C_{\mathrm{LNT}}$, giving the following driving impedance:

$$Z_{\mathrm{EQS}} = \frac{1}{(1-j)C_{\mathrm{LNT}}f_0} = \frac{(1+j)}{2C_{\mathrm{LNT}}f_0}. \tag{1}$$

Z_{EQS} corresponds to a complex resistance (i.e., there is a complex relation between the current and the voltage in the time domain). The real part comes from the charge sampled by C_{LNT} in the I path, while the imaginary part comes from the charge sampled in the Q path.

Fig. 5(b) reports the final model for the I (Q) path. Again, the down-conversion gain versus frequency is obtained from the partition of the down-converted current signal $I_{\mathrm{IN,BB}}$ between the driving and the BB impedance. The presence of a complex value element (resistor) makes the STF asymmetric around dc. This behavior captures the asymmetry around the LO of the RF transfer function (different gains for frequencies below and above f_0) already reported in the literature [1], [4]–[6].

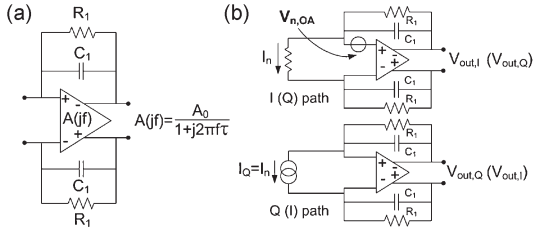

Fig. 6. (a) TIA used as BB load. (b) OA noise model.

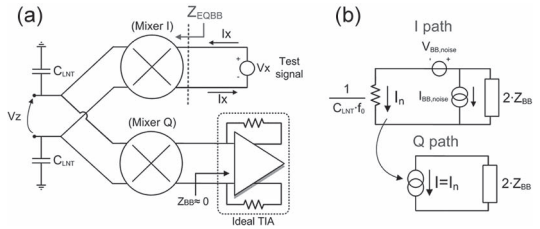

Fig. 7. (a) Impedance test for BB noise. (b) BB noise quadrature-chain model.

As an example, we consider for the BB a TIA based on a finite-bandwidth operational amplifier (OA) that implements a first-order filter at $1/(R_1C_1)$, as shown in Fig. 6(a). The down-conversion current gain $G(jf)$ (i.e., the ratio between the current into $Z_{\rm BB}$ and the RF current) obtained using a normalized complex RF tone (phasor) $I_{\rm IN,RF}=\exp(j2\pi f_{\rm RF}t)$ at frequency $f_{\rm RF}=f_0+f$ is

$$G(jf)=\frac{\frac{\sqrt{2}}{\pi}\cdot\frac{(1+j)}{4C_{\rm LNT}f_0}}{\frac{(1+j)}{4C_{\rm LNT}f_0}+\frac{R_1(1+j2\pi f\tau)}{(1+j2\pi fC_1R_1)(1+A_0+j2\pi f\tau)}}. \quad (2)$$

The equivalent impedance $Z'_{\rm EQS}$, for $R_{\rm SW}\neq 0$ and for a finite resistance $R_{\rm LNT}$ in parallel to $C_{\rm LNT}$ at the LNT output, is computed in Appendix B, making use of the result in Appendix A. Applying this result for the same BB as above, the following STF is obtained:

$$G(jf)=\frac{1}{1+j2\pi f_{\rm RF}C_{\rm LNT}R_{\rm SW}}\cdot\frac{\frac{\sqrt{2}}{\pi}\cdot\left(\frac{Z_{\rm EQS'}}{2}\right)}{\left(\frac{Z_{\rm EQS'}}{2}\right)+\frac{R_1(1+j2\pi f\tau)}{(1+j2\pi fC_1R_1)(1+A_0+j2\pi f\tau)}} \quad (3)$$

(neglecting $R_{\rm LNT}$ in the first factor). Comparing the analytical model with simulation, we have verified that, for the latter case, (3) is more accurate than the STF provided in [5] and [6]. On the other hand, the SC model cannot handle much more complicated RF loads like those considered in [5].

IV. 25%-D-C Quadrature-Chain Noise Model

The following analysis is divided into two parts: BB noise and mixer switch noise.

A. BB Noise Model

The main difference with the STF situation is that, now, to compute the driving impedance of the I (Q) path, the correlated test signal on the Q (I) path has to be substituted with $Z_{\rm BB}$. Therefore, the driving impedance is no more independent from $Z_{\rm BB}$ as it was for the STF. To simplify calculations, an ideal TIA (i.e., $Z_{\rm BB}=0$) is assumed [Fig. 7(a)]. This implies that, when $C_{\rm LNT}$ is connected to the Q path, it is fully discharged. For a real BB, this simplification introduces an error in the model, whose magnitude will be given later.

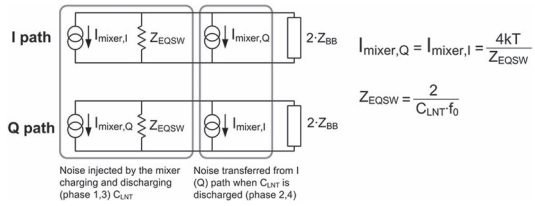

Fig. 8. Mixer switch noise quadrature-chain model.

For this case, a real driving impedance $Z_{\rm EQBB}=1/(C_{\rm LNT}\cdot f_0)$ results. Moreover, since, in each clock cycle, the I (Q) noise stored in $C_{\rm LNT}$ is discharged in the Q (I) path, the noise originating from the I (Q) path is also observed in the Q (I) path ($I-Q$ noise crosstalk). The obtained BB noise model is shown in Fig. 7(b). Notice that $Z_{\rm EQBB}$ (the noise driving impedance) is 3 dB larger (in modulus) than $Z_{\rm EQS}$ (the STF driving impedance), but an additional noise source is present in the Q path.

The model is now applied to the same BB used in the STF section [Fig. 6(b)]. The noise PSD at the I (Q) TIA differential output $V_{{\rm out},I}$ $(V_{{\rm out},Q})$ produced by the I (Q) OA is

$$\frac{dV^2_{{\rm out},I}}{df}=4kTR_{\rm OA}\cdot\left|\frac{A(jf)}{A(jf)+1}\cdot\frac{R_1+(Z_{\rm EQBB}/2)+j2\pi fR_1C_1(Z_{\rm EQBB}/2)}{\frac{R_1}{A(jf)+1}+(Z_{\rm EQBB}/2)+j2\pi R_1C_1(Z_{\rm EQBB}/2)}\right|^2 \quad (4)$$

and the noise PSD produced by the Q (I) OA is

$$\frac{dV^2_{{\rm out},I}}{df}=4kTR_{\rm OA}\cdot\left|\left(\frac{A(jf)}{A(jf)+1}\right)^2\cdot\frac{R_1}{\frac{R_1}{A(jf)+1}+(Z_{\rm EQBB}/2)+j2\pi R_1C_1(Z_{\rm EQBB}/2)}\right|^2 \quad (5)$$

in which $R_{\rm OA}$ is the equivalent input noise resistance of the OA (either of the I and Q paths).

B. Mixer Switch Noise Model

The noise produced by the switching transistors is analyzed following the approach proposed in [9] and extending it to the quadrature case. For simplicity, an ideal TIA is again assumed at BB $(Z_{\rm BB}=0)$.

The $I-Q$ noise crosstalk is relevant also in this case. Each switch in the I (Q) path (when on) injects its noise directly into the I (Q) BB on one side and into $C_{\rm LNT}$ on the other side. The amount of noise charge sampled by $C_{\rm LNT}$ at turnoff depends on the $R_{\rm SW}-C_{\rm LNT}$ time constant and on the clock on-time. This noise charge is then discharged into the Q (I) BB during the next LO phases, contributing to the overall RX noise. Due to the symmetry of the architecture when $Z_{\rm BB}=0$, mixer I (Q) divides its noise evenly between the two paths. For the I (Q) BB and assuming that $1/(2\pi R_{\rm SW}C_{\rm LNT})\gg f_0$, both mixers I (Q) and Q (I) contribute a noise equal to that of an equivalent SC noise resistance $Z_{\rm EQSW}=2/(C_{\rm LNT}\cdot f_0)$ as shown in Fig. 8.

Applying again the model to the BB used in the STF section, the noise PSD contributed by either the I or Q mixer at the I (Q) TIA differential output $V_{{\rm out},I}$ $(V_{{\rm out},Q})$ is

$$\frac{dV^2_{{\rm out},I}}{df}=\frac{4kT}{Z_{\rm EQSW}}\cdot\left|\frac{A(jf)}{A(jf)+1}\cdot\frac{R_1Z_{\rm EQSW}}{\frac{R_1}{A(jf)+1}+(Z_{\rm EQSW}/2)+j2\pi fR_1C_1(Z_{\rm EQSW}/2)}\right|^2. \quad (6)$$

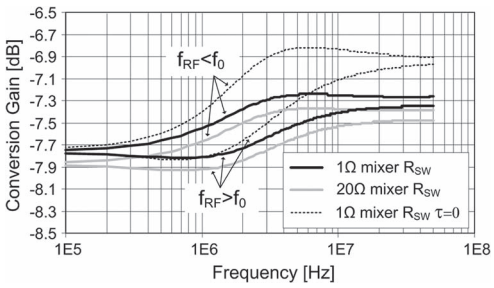

Fig. 9. Down-conversion mixer gain (STF) ($R_{\rm LNT} = 2$ kΩ).

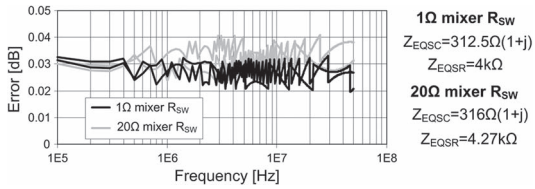

Fig. 10. Spectre PAC versus STF model ($C_{\rm LNT} = 400$ fF and $R_{\rm LNT} = 2$ kΩ).

TABLE I
PSS–PAC SIMULATIONS VERSUS STF MODEL

RF load [fF-kΩ]	800-2		800-0.25		400-2		400-0.25		100-2		100-0.25	
R_{SW} [Ω]	1	20	1	20	1	20	1	20	1	20	1	20
Max Error [mdB]	85	95	78	90	43	40	50	58	8	22	70	80

V. MODEL VERSUS SIMULATIONS

The comparison with simulations will be done only for the quadrature architecture (i.e., the most used in practice) and placing at BB the TIA shown in Fig. 6(a). The simulations are performed using Spectre PSS–PAC-PNOISE (PSS harmonics = 100; PNOISE sidebands = 100). Except for the mixer noise, all simulations use simplified switches (i.e., without parasitics). The LO frequency is 2 GHz and the value of $C_{\rm LNT}$ is 400 fF.

A. STF

The simulated down-conversion gain versus frequency at the I (Q) output for $R_1 = 5$ kΩ, $C_1 = 15$ pF (2.1-MHz pole), $A_0 = 10^2$, and $\tau = 31.8$ ns (500-MHz OA bandwidth) is reported in Fig. 9. The four solid curves represent the down-conversion gains for $f_{\rm RF} > f_0$ and $f_{\rm RF} < f_0$ for the cases of $R_{\rm SW} = 1\ \Omega$ and $R_{\rm SW} = 20\ \Omega$. To get a quantitative feel for the accuracy of the model, the difference between the simulated and the analytical predicted conversion gain (3) is plotted in Fig. 10 versus frequency. The four curves correspond again to the positive and negative frequency offsets from f_0 for $R_{\rm SW} = 1\ \Omega$ and $R_{\rm SW} = 20\ \Omega$. The values of the equivalent driving impedances (single ended) are also shown in the figure. The model correctly predicts the asymmetry in the conversion gain between positive and negative frequencies around the LO. Table I reports the maximum error when $C_{\rm LNT}$ is varied from 100 to 800 fF and $R_{\rm LNT}$ is varied from 250 Ω to 2 kΩ. The error is within 0.1 dB in the whole 50-MHz frequency range. The consistently small error for such a large variation of the parameters proves the solidity of the model. The model has shown comparable accuracy also with low RF impedance and a pure capacitor as $Z_{\rm BB}$, i.e., it can also predict a voltage-mode STF. Instead, the model does not work if a purely resistive $Z_{\rm BB}$ is chosen, since point 2 in Section II is not satisfied.

The gain frequency dependence (Fig. 9) can be intuitively understood noting that it is maximum at high frequency where $Z_{\rm BB}$ is minimum and minimum near dc where $Z_{\rm BB}$ is maximum. The pole of $Z_{\rm BB}$ makes the gain increase, while its zero (due to the finite OA bandwidth) makes it flatten again. To better understand the gain behavior, the dashed curves in Fig. 9 refer to the simple case of $\tau = 0$ and $R_{\rm SW} = 1\ \Omega$. In this case, $Z_{\rm BB}$ decreases monotonically with frequency, and when it becomes sufficiently small, no current partition can occur so that the ideal -6.9-dB ($\sqrt{2}/\pi$) conversion gain is reached.

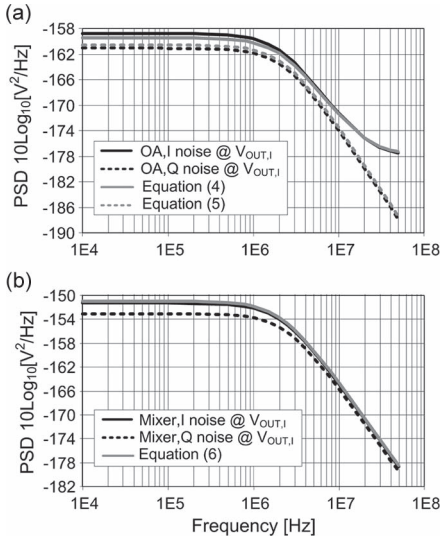

Fig. 11. (a) BB noise PSDs. (b) Mixer noise PSDs. Spectre PNOISE versus model.

B. BB Noise and Mixer Switch Noise

The simulated noise PSDs due to the I and Q OAs at the I TIA differential output $V_{{\rm out},I}$ are reported in Fig. 11(a) from dc to 50 MHz for $R_{\rm SW} = 20\ \Omega$ and the same parameters in the previous section. Equations (4) and (5) are also plotted in Fig. 11(a) to compare them with the simulated results. The noise PSDs obtained from the model fit the simulation with good precision. The in-band (2-MHz) integrated errors are -0.6 and $+0.5$ dB, respectively. Summing the in-band output noise values (in an uncorrelated way) for the I and Q OAs gives -0.15-dB total error. This value remains quite low even when $C_{\rm LNT}$ is varied from 100 to 800 fF (-0.27 and -0.12 dB, respectively). The error is due to the fact that zero BB impedance in the Q (I) path has been assumed in the model. In actuality, near dc, the BB input impedance reaches its maximum value $R_1/(1 + A_0)$, giving rise to a charge loss in the noise crosstalk effect described in Section IV-A. This charge loss is responsible for the incorrect noise redistribution between the I and Q paths. Notice that, at high frequency, the PSD error tends to zero since the BB input impedance approaches zero.

Consider now the switching transistor noise. The simulated PSDs at the I TIA differential output $V_{{\rm out},I}$ due to either the I or Q mixer are shown in Fig. 11(b) for the parameters as above. Real switching transistors have been used in this simulation, i.e., $R_{\rm SW} = 20\ \Omega$, and parasitics have been included. Equation (6) is plotted also in Fig. 11(b) for comparison (including the switch parasitic capacitance into $C_{\rm LNT}$). For the I mixer noise, the model fits the simulation with good precision (0.25-dB in-band integrated error). The bigger error for the Q mixer noise is explained again by the ground discharging approximation used in the model.

If the noise due to the mixers is computed when $C_{\rm LNT}$ is varied from 100 to 800 fF, the integrated in-band error varies

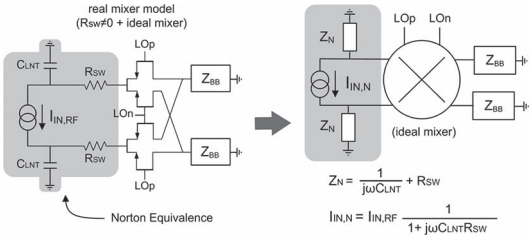

Fig. 12. Finite switch on-resistance $R_{\rm SW}$. Norton equivalence.

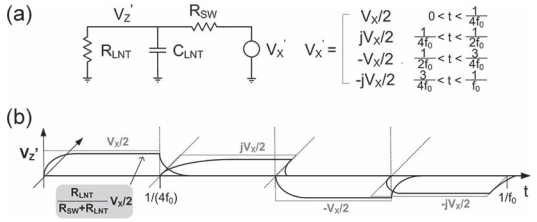

Fig. 13. General impedance analysis for finite $R_{\rm LNT}$ and $R_{\rm SW} \neq 0$. (a) Equivalent circuit used in the impedance test. (b) Voltage across $C_{\rm LNT}$.

from 0.1 to 0.3 dB for the I path and from 0.8 to 3 dB for the Q path. Summing the in-band noise values (evaluated at the output and in an uncorrelated way) of the I and Q sources gives a total error that varies from 0.5 to 1.5 dB. At high frequency, the PSD error again tends to zero, and the 50% I/Q noise partition is verified. Notice that the error becomes significant (>1 dB) only for values of $C_{\rm LNT}$ much larger than practical ones (generally less than 0.5 pF) and having assumed a TIA in-band input impedance of 50 Ω, which is a very pessimistic value.

As opposed to the STF model, the noise model cannot correctly represent the behavior of either the mixer or the BB over the entire frequency range if a pure capacitor is used at BB [1], [2]. In this case, the model is valid only beyond the frequency at which $Z_{\rm BB}$ becomes sufficiently low with respect to $Z_{\rm EQBB}$.

Appendix A
Simplifying Assumptions of the Model

A. Nonideal Switch and LO

Section II makes two simplifying assumptions, i.e., $R_{\rm SW} = 0$ and ideal LO phases. It turns out that removing the first one also removes the second since it is possible to demonstrate that the presence of overlap or disoverlap can be described (with an acceptable error) with an equivalent nonzero $R_{\rm SW}$.

If $R_{\rm SW} \neq 0$, it is no longer possible to directly separate $I_{\rm IN}$ from $C_{\rm LNT}$ at RF (doubling the number of mixers), but an intermediate step is required as shown in Fig. 12. First, the real mixer is converted into a cascade of a resistance $R_{\rm SW}$ (placed on its RF side) and an ideal mixer with $R_{\rm SW} = 0$ [3]. Second, the RF circuit is substituted with its parallel Norton equivalent. The equivalence is valid under the assumption of a constant $R_{\rm SW}$ during the on-period, which makes the circuit linearly time invariant. The RF current generator can then be down-converted and substituted with its BB equivalent. The conversion gain from $I_{\rm IN,RF}$ to $I_{\rm IN,BB}$ is still equal to $2/\pi$ at a low frequency but shows a low-pass shape. However, for typical values of $R_{\rm SW}$, the effect is negligible for f comparable with f_0. On the other hand, the value of the impedance seen at BB is affected by the presence of $R_{\rm SW}$, as discussed in the next section.

B. $Z_{\rm EQS}$ for a Finite Resistance $R_{\rm LNT}$ and $R_{\rm SW} \neq 0$: $Z'_{\rm EQS}$

When a finite resistance $R_{\rm LNT}$ is placed in parallel with $C_{\rm LNT}$, a simple SC theory cannot be directly applied. The STF is obtained as in Section III; however, $Z_{\rm EQS}$ is computed in the current domain referring to Fig. 13(a) and assuming also that $R_{\rm SW} \neq 0$ and 25% D-C.

The voltage across $C_{\rm LNT}$ [V'_Z in Fig. 13(a)] during each clock phase has an exponential response [Fig. 13(b)] to the input test voltage V'_X. The average current flowing into $C_{\rm LNT}$ is given by the charge stored in it times the LO frequency and depends only on the value of V'_Z at the end of the phase. On the other hand, the average $R_{\rm LNT}$ current is obtained, integrating $I_{\rm RLNT} = V'_Z/R_{\rm LNT}$ in the same phase and observing that only half of the phases have to be considered in the evaluation. Separating the contributions, the differential BB impedances due to $C_{\rm LNT}$ and $R_{\rm LNT}$ are

$$Z_{\rm EQSC} = \frac{(1+j)}{2C_{\rm LNT}f_0} \cdot \frac{R_{\rm LNT}+R_{\rm SW}}{R_{\rm LNT}} \cdot \left(1 - e^{\left(\frac{1}{4Tf_0}\right)}\right) \quad (7)$$

$$Z_{\rm EQSR} = 4(R_{\rm LNT}+R_{\rm SW}) \cdot \frac{1}{\left(1 - 4Tf_0 + 4Tf_0 e^{-\left(\frac{1}{4Tf_0}\right)}\right)} \quad (8)$$

respectively, where T is the time constant of the $R_{\rm SW}\|R_{\rm LNT}-C_{\rm LNT}$ network. The equivalent BB differential impedance $Z'_{\rm EQS}$ is the parallel of $Z_{\rm EQSC}$ and $Z_{\rm EQSR}$ and can be used to get the mixer STF by current partition, as explained in Section III.

When $R_{\rm SW} = 0$, $Z_{\rm EQSC}$ corresponds to $Z_{\rm EQS}$ (as expected), and $Z_{\rm EQSR}$ is equal to $4R_{\rm LNT}$. The latter result can be understood noting that $R_{\rm LNT}$ is seen from BB, during each LO period, for a time equal to $1/(4f_0)$; therefore, its value is multiplied by four. $Z_{\rm EQSC} = Z_{\rm EQS}$ is also true if $R_{\rm SW} \neq 0$, but $R_{\rm LNT}$ is infinite, under the assumption that the network settles completely within the 25%-D-C time slot.

References

[1] C. Andrews and A. C. Molnar, "Implications of passive mixer transparency for impedance matching and noise figure in passive mixer-first receivers," *IEEE Trans. Circuits Syst. I, Reg. Papers*, vol. 57, no. 12, pp. 3092–3103, Dec. 2010.

[2] M. C. M. Soer, E. A. M. Klumperink, P.-T. de Boer, F. E. van Vliet, and B. Nauta, "Unified frequency-domain analysis of switched-series-RC passive mixers and samplers," *IEEE Trans. Circuits Syst. I, Reg. Papers*, vol. 57, no. 10, pp. 2618–2631, Oct. 2010.

[3] H. Khatri, P. S. Gudem, and L. E. Larson, "Distortion in current commutating passive CMOS downconversion mixers," *IEEE Trans. Microw. Theory Tech.*, vol. 57, no. 11, pp. 2671–2681, Nov. 2009.

[4] A. Mirzaei, H. Darabi, J. C. Leete, X. Chen, K. Juan, and A. Yazdi, "Analysis and optimization of current-driven passive mixers in narrowband direct-conversion receivers," *IEEE J. Solid-State Circuits*, vol. 44, no. 10, pp. 2678–2688, Oct. 2009.

[5] A. Mirzaei, H. Darabi, J. C. Leete, and Y. Chang, "Analysis and optimization of direct-conversion receivers with 25% duty-cycle current-driven passive mixers," *IEEE Trans. Circuits Syst. I, Reg. Papers*, vol. 57, no. 9, pp. 2353–2366, Sep. 2010.

[6] A. Mirzaei and H. Darabi, "Analysis of imperfections of 4-phase passive-mixer-based high-Q bandpass filters in SAW-less receivers," *IEEE Trans. Circuits Syst. I, Reg. Papers*, vol. 58, no. 5, pp. 879–892, May 2011.

[7] E. Sacchi, I. Bietti, S. Erba, L. Tee, P. Vilmercati, and R. Castello, "A 15 mW, 70 kHz 1/f corner direct conversion CMOS receiver," in *Proc. IEEE CICC*, 2003, pp. 459–462.

[8] W. Redman-White and D. M. W. Leenaerts, "1/f noise in passive CMOS mixers for low and zero IF integrated receivers," in *Proc. IEEE ESSCIRC*, 2001, pp. 41–44.

[9] S. Chehrazi, A. Mirzaei, and A. A. Abidi, "Noise in current-commutating passive FET mixers," *IEEE Trans. Circuits Syst. I, Reg. Papers*, vol. 57, no. 2, pp. 332–344, Feb. 2010.